

# Nanoparticle release quantification during weak and intense dry dispersion of nanostructured powders

**Daniel Göhler and Michael Stintz**

Research Group Mechanical Process Engineering, Institute of Process Engineering and Environmental Technology, Technische Universität Dresden, D-01062 Dresden, Germany.

E-mail: daniel.goehler@tu-dresden.de

**Abstract.** Currently, the characterisation of particle release from nanostructured powders is realised based on different release scenarios, which were typically designed to describe real powder handling processes. Most of these scenarios base on short term stress situations (e.g. drop down, mixing) and are thus accompanied with dynamic changes of the particle number concentration, which complicates both the process characterisation and the release characterisation. In this study, two continuous release processes for weak and intense dispersion of powder agglomerates were analysed based on considerations regarding energetic and instrumental impact.

## 1. Introduction

Nanostructured powders are the basic components of numerous nano-products and were thus the subject of several particle release investigations for risk estimation [1]. Performed studies examined different dispersion procedures, which can be classified to the acting stress intensity level. Three groups may be distinguished: drop down procedures [2-5], fluidized bed approaches [6-8] and high energy dispersion treatments [9].

The amount of the dispersion energy affects both the particle size distribution (PSD) and the particle number concentration (PNC) and can thus lead for one powder to a large data diversity regarding the particle release. Typical release scenarios for powder handling are short term stress situation (e.g. drop down, mixing), which lead in most cases to dynamic changes on the particle release that complicates tasks regarding the basic process characterisation or the selection of suitable measurement devices. This in turn limits the comparability among the results of different release studies.

This paper aims at a uniform methodological approach to the quantification of (nano)-particle release from dry powder due to weak and intense dispersion processes. These processes are intended to provide a time-constant release signal, as is already feasible with commercial aerosol generators for intense dispersion like the well-known rotating brush generator (RBG). A new release process was developed that ensures time-constant size and concentration values due to weak dispersion. The so-called weak dispersion unit (WDU) was designed by considering previous experiences and the possible impact of analytic instrumentation on the state of dispersion, i.e. the measurement results.



## 2. Characteristics of dispersion processes

### 2.1. Technical power/energy consumption

Today it is common practise to quantify the progress of dispersion via any kind of technical power or energy input into the dispersed system, i.e. an indirect but measureable or accessible power/energy input of the operated disperser.

For example, wet dispersion processes by ultrasonication are frequently described by the volume-specific calorimetric energy input  $e_{V,CAL}$  based on the calorimetric power  $P_{CAL}$  related to the suspension volume  $V_{SUS}$  and dispersion duration  $t_{DIS}$  [10]:

$$e_{V,CAL} = \frac{P_{CAL} \cdot t_{DIS}}{V_{SUS}} = \left( \frac{m_F \cdot c_p \cdot \Delta T}{t} \right) \cdot \frac{t_{DIS}}{V_{SUS}} \quad (1)$$

In contrast to  $e_{V,CAL}$  employed for wet dispersion, the mass-specific pneumatic energy consumption  $e_{M,PNE}$  based on the pneumatic power  $P_{PNE}$  and the supplied powder mass flow could be used for describing dry dispersion processes [11,12]:

$$e_{M,PNE} = \frac{P_{PNE}}{\dot{m}_p} = (Q \cdot \Delta p) \frac{1}{\dot{m}_p} \quad (2)$$

The pressure drop  $\Delta p$  is affected by the acceleration of the particles within the volumetric air flow  $Q$ , and also by the geometry of the piping system. The pressure drop due to particle acceleration is often too low for measurement, whereas the geometric-based one differs considerably among existing devices. Thus, there is a need for additional characteristic parameters for dry dispersion processes.

### 2.2. Dispersion stress

Powder dispersion usually relies on several interacting forces (resulting from drag, inertia, gravity, impacts, etc.), which act on the particles/agglomerates and cause tension, compression, bending and shear. This results in deagglomeration, i.e. agglomerate erosion and/or fragmentation [13], when the corresponding stresses exceed the agglomerate strength:

$$\sigma_{STRENGTH} < \sigma_{STRESS} \quad (3)$$

A comparison of existing dispersion models [11, 14-17] shows that tensile stress caused by particle acceleration dominates the dispersion of submicron agglomerates in air flows at similar and low particle load ( $< 0.1$  vol.-%). Hence, the decisive parameter for pneumatic dispersion is then the maximum relative velocity  $v_{rel,max}$  between the undisturbed air flow and the particle within the dispersion unit.

In order to demonstrate this statement, three different commercial aerosol generators (see Table 1) were operated with two test powders (see Table 3) at comparable low powder feeding (powder flow rate of  $30 \text{ mm}^3 \cdot \text{min}^{-1}$ ).

**Table 1.** Commercial aerosol generators operated for statement demonstration.

		RBG 1000	RODOS	SAG 410/U
manufacturer	[-]	Palas GmbH, Karlsruhe, Germany	Sympatec GmbH, Clausthal-Zellerfeld, Germany	Topas GmbH, Dresden, Germany
dispersion unit	[-]	dispersion cover type A	ejector	ISO-injector (ISO 5011)
$A_{DIS}^a$	[mm <sup>2</sup> ]	18.5	32.9	12.6
$Re^b$	[-]	$8.8 \cdot 10^3 - 2.8 \cdot 10^4$	$1.0 \cdot 10^4 - 2.1 \cdot 10^4$	$6.2 \cdot 10^3 - 1.4 \cdot 10^4$
reference		[18]	[19]	[20]

<sup>a</sup>... dispersion cross section used for the calculation of maximal air velocity

<sup>b</sup>... Reynolds number for the analysed system pressure range (0.5 bar - 3.5 bar)

The corresponding number-weighted PSDs ( $PSD_0$ ) were measured by means of an electrical mobility spectrometer (SMPS, Model 3934, TSI Inc., USA) after sufficient dilution and bipolar neutralisation within a flow channel.

Figure 1 a shows determined agglomerate number median diameters  $x_{50,0}$  of the analysed two test powders over the system pressure, whereas Figure 1 b gives  $x_{50,0}$  over  $v_{rel,max}$ .

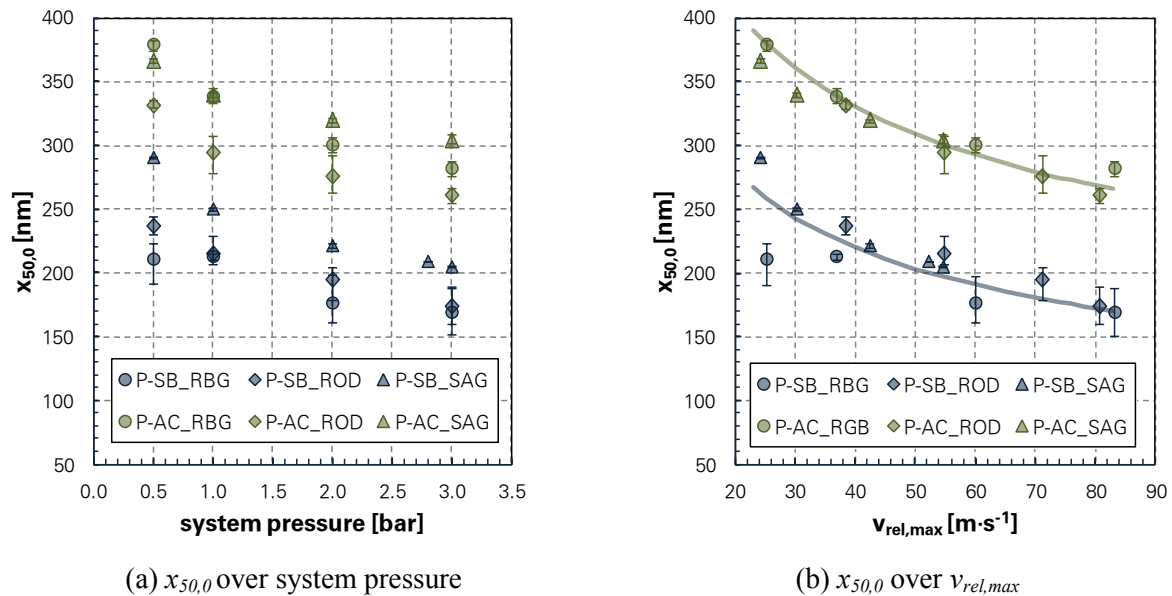


**Figure 1.** Progress of dry powder dispersion for 3 different aerosol generators (RBG, ROD, SAG) and two filter test powders (P-SB, P-AC) at similar powder feeding as function of system pressure (a) and  $v_{rel,max}$  (b).

It is evident, that  $v_{rel,max}$  is more appropriate to compare the progress of dry powder dispersion than the typical used system pressure or the volumetric aerosol flow (not shown here). According to this, the agglomerate number median diameter  $x_{50,0}$  of powder dispersion is a function of  $v_{rel,max}$ :

$$x_{50,0} = f(v_{rel,max}) \quad (4)$$

### 2.3. Conclusion for the design of weak dispersion test-scenarios

The relationship for  $x_{50,0}$  was the basis for our considerations regarding the design of a suitable test scenario. Additionally, attention has to be paid also to the employed aerosol measurement instruments, which have often critical zones where a post-dispersion of airborne agglomerates is possible. Such zones are particle separators at the inlet (e.g. impactors, aerocyclones), bends and constrictions (e.g. nozzles) in the piping system or the measurement zone. Table 2 provides approximated values of  $v_{rel,max}$  for typical operation conditions of selected aerosol measurement instruments.

**Table 2.** Estimation of  $v_{rel,max}$  within common used aerosol measurement instruments.

instrument [-]	critical zones [-]	volumetric flow [L·min <sup>-1</sup> ]	inner diameter [mm]	$v_{rel,max}$ [m·s <sup>-1</sup> ]
aerodynamic particle sizer (APS)	staged acceleration nozzle	1.0 to 5.0	0.81 to 1.04	≈ 60
scanning mobility particle sizer (SMPS)	inlet impactor	0.3	4.5 to 0.71	≈ 12.3
			4.5 to 0.46	≈ 30.2
condensation particle counter (CPC)	bends	0.3	4.5	≈ 0.3

It is obvious that  $v_{rel,max}$  in the instruments must not exceed that of the intended dispersion process. Otherwise particle characterisation would solely reflect the post-dispersion within the measurement instrument. Moreover, since losses of coarse agglomerates in the experimental setup are unavoidable and measures of dilution are mandatory, the particle mass flow through the critical zones of the instruments is considerable lower than the stressed particle mass flow by the simulated process. Consequently, the process should warrant considerably higher  $v_{rel,max}$  than those prevailing in the analytical instruments.

### 3. Experimental details for the characterisation of particle release

#### 3.1. Materials

Different types of powders were used within this study for dry dispersion process characterisation and particle release characterisation (see Table 3). Two typical filter test powders (P-SB, P-AC) were employed for the characterisation of the dispersion process (see subchapter 2.2).

**Table 3.** Materials of interest: identification key of analysed powders; data on bulk density and compacted apparent density (for operation of RBG).

Powder		Pural SB	AC Fine 2 <sup>a)</sup>	Iron oxide pigment, transparent			Iron oxide pigment, opaque		
batch	[-]	A	A	A	B	C	A	B	C
sample ID	[-]	P-SB-A	P-AC-A	P-TE-A	P-TE-B	P-TE-C	P-DE-A	P-DE-B	P-DE-C
$\rho_{bulk}$	[kg·m <sup>-3</sup> ]	794	764	779	756	754	695	690	670
$\rho_{comp}$	[kg·m <sup>-3</sup> ]	872	1515	889	902	892	1615	1609	1439
$k_{POW}$ <sup>b)</sup>	[-]	0.09	0.50	0.12	0.16	0.16	0.57	0.57	0.53
water content	[%]	2.98	0.03	1.70	1.31	1.46	0.06	0.07	0.07
BET	[m <sup>2</sup> ·g <sup>-1</sup> ]	250	n.a.	85	85	85	n.a.	n.a.	n.a.

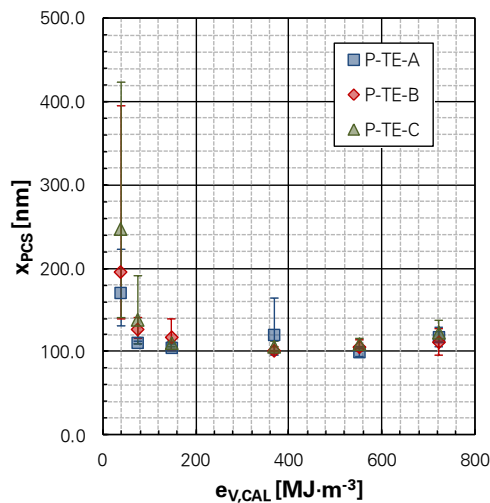
<sup>a)</sup> ... Arizona test dust type ISO 12103-A2 with 68-76 wt.-% SiO<sub>2</sub> and 10-15wt.-% of Al<sub>2</sub>O<sub>3</sub>

<sup>b)</sup> ... powder compressibility based on  $\rho_{bulk}$  and  $\rho_{comp}$

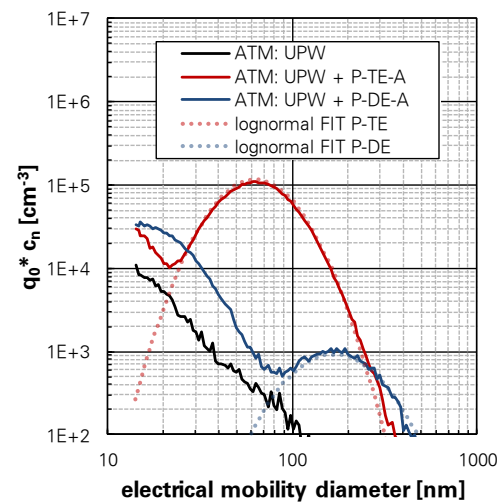
Beside the test powders, two iron oxide pigments, a nanostructured one (P-TE) and a non-nanostructured one (P-DE), were focused for release characterisation. The former pigment is the same as used in [21]. In order to estimate the influence of sample age, three different batches (A, B, C) were analysed for each pigment.

To approximate the PSD<sub>0</sub> with those of the smallest dispersible units for very intense dispersion, wet dispersion series were performed by ultrasonication (UDS 751/S7, Topas GmbH, Germany) in combination with dynamic light scattering (HPPS 5002, Malvern Instruments GmbH, Germany) for different  $e_{V,CAL}$  according to eq. 1 with  $P_{CAL,UDS}(P_{EL} = 100 \%, V_{AQU} = 50 \text{ mL}) = 31 \text{ W}$ .

The aqueous suspensions at  $e_{V,CAL} = 367 \text{ MJ} \cdot \text{m}^{-3}$  were then aerosolized (ATM 220, Topas GmbH, Germany) and dried to determine the corresponding PSD<sub>0</sub> by an electrical mobility aerosol spectrometer (SMPS, Model 3938, TSI Inc., Shoreview, USA). As typical for this procedure, salt crystals of the pure dispersion medium (ultrapure water at 18.3 MΩ, UPW) were already measurable. To distinguish the fraction of salt crystals from the pigments, a data fitting was performed assuming a lognormal density distribution (see Figure 2). According to this, the approximated PSD<sub>0</sub> of smallest dispersible units of the nanostructured pigment P-TE can be described by  $x_{50,0} = 63 \text{ nm}$ ,  $\sigma_{ln} = 0.43$  with  $Q_0(100 \text{ nm}) = 86 \%$ , the one for the non-nanostructured P-DE by  $x_{50,0} = 168 \text{ nm}$ ,  $\sigma_{ln} = 0.49$  with  $Q_0(100 \text{ nm}) = 15 \%$ .



(a) wet dispersion series on P-TE



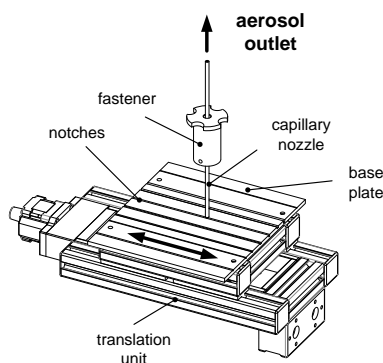
(b) aerosolized and dried suspensions

**Figure 2.** Mean intensity-weighted particle size  $x_{PCS}$  of P-TE over  $e_{V,CAL}$  (a) and  $PSD_0$  of the aerosolized suspensions at  $e_{V,CAL} = 367 \text{ MJ} \cdot \text{m}^{-3}$  with fitted log-normal density distribution (b).

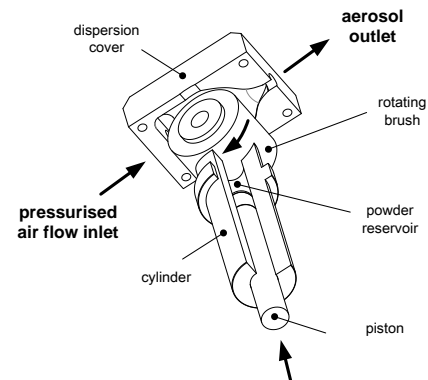
### 3.2. Instrumentation

**3.2.1. Dry dispersion systems.** Two different test-scenarios were examined within this study for a quantitative release characterisation. The intense dispersion system is based on a commercial rotation brush generator (RBG 1000, Palas GmbH, Germany), whereas for the low energetic consideration a weak dispersion unit (WDU) was developed that offers continuous powder feeding and low but adjustable dispersion energy input.

The WDU (Figure 3 a) consists of the linear-driven translation unit as described in [22]. A base plate with notches of different geometries and dimensions serves for the purpose of continuous volumetric powder feeding. The powder removal from the notch and the dispersion process is achieved by a stain-less steel capillary suction nozzle arranged 0.5 mm above the notch. Due to the separation of the dosing system from the dispersion system, the supplied volumetric powder flow and the dispersion intensity can be varied independently. Within this study, the WDU was operated at a volumetric powder flow rate of  $30 \text{ mm}^3 \cdot \text{min}^{-1}$  and  $v_{rel,max} \approx 25 \text{ m} \cdot \text{s}^{-1}$  ( $P_{PNE,WDU}(4.6 \text{ L} \cdot \text{min}^{-1}) = 0.2 \text{ W}$ ). The process parameters were chosen with respect to the operating conditions of the measurement devices as discussed in subchapter 2.3.



(a) WDU operation principle



(b) sectional view of the RBG dispersion unit

**Figure 3.** Operated dispersion units for the characterisation of particle release from powders due to weak and intense dry dispersion of powder agglomerates.

The RBG consists of a cylinder-piston-system for a constant powder feeding into a rotating brush (Figure 3 b). The brush transports the powder into the dispersion cover, where the actual dispersion process is caused by a pressurised air flow [18]. The RBG was operated with dispersion cover type A at a dispersion pressure of 3.5 bar ( $v_{rel,max} \approx 100 \text{ m}\cdot\text{s}^{-1}$ ), a powder flow of  $25.7 \text{ mm}^3\cdot\text{min}^{-1}$  and a rotational steel brush frequency of  $1210 \text{ min}^{-1}$  ( $P_{PNE,RBG}(3.5\text{bar}) \approx 134 \text{ W}$ ). Note, the lower the system pressure is during RBG operation, the higher is the relative impact of mechanical stress by the rotating brush during dry powder dispersion.

**3.2.2. Particle measuring instruments.** The generated aerosols were analysed from the nanoscale up to the microscale using a condensation particle counter (CPC, Model 3022A, TSI Inc., USA), an electrical mobility aerosol spectrometer (SMPS, Model 3938, TSI Inc., USA) and a time-of-flight spectrometer (APS, Model 3321, TSI Inc. USA).

To avoid post-dispersion and re-entrainment of agglomerates during the analyses with the WDU, the SMPS was operated without inlet impactor. Furthermore, SMPS-data were evaluated without multiple charge correction (MCC) for both release scenarios. The occasional high fractions of large particles outside the SMPS detection limit (see Figure 7) would otherwise lead to considerable artefacts in the curve shapes. Note, that the omission of the MCC leads to finer PSD<sub>0</sub>s and higher PNCs as present [25]. Based on the absence of detailed information regarding the effective agglomerate density, the given APS-data were evaluated without Stokes correction. In the case of WDU dispersion, a post-dispersion within the APS acceleration nozzle could not be ruled out. The most robust results based on the determined PNC measured by the CPC.

### 3.3. Experimental setups and procedures

**3.3.1. WDU setup.** The experimental setup that was operated for the characterization of the WDU-induced particle release is shown in Figure 4. The experimental setup was operated within a laminar flow bench (Model LF-VM-K0615, STEAG Laminarflow Prozesstechnik GmbH, Germany) to avoid particle contamination from the background.

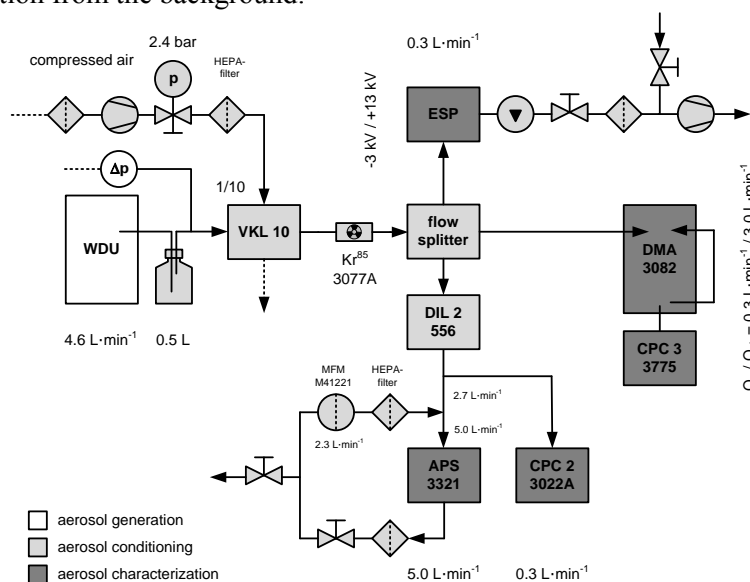


**Figure 4.** Experimental setup for weak dry powder dispersion by operating the WDU.

The aerosols generated by the capillary tube were firstly passed through a 0.5 L compensation tank to decrease fluctuations in PNC and to deposit surviving coarse agglomerates. The suction flow through the nozzle and the compensation tank was realized by a compressed air driven dilution unit

(Model VKL10, Palas GmbH, Germany), which served furthermore for a defined pre-dilution and a pressure-compensated aerosol sampling. All measuring devices received their aerosol sample through a flow splitter. An additional dilution system (Model DIL 556, Topas GmbH, Germany) was placed before APS and CPC. The sample flow of the APS was generally post-diluted by partial back-mixing with HEPA-filtered device exhaust. During the analyses, a mean relative humidity of  $19.5\% \pm 3.3\%$  and a mean temperature of  $25.0^\circ\text{C} \pm 1.2^\circ\text{C}$  were logged.

**3.3.2. RBG setup.** The experimental setup that was operated for the characterisation of the RBG-induced particle release is shown in Figure 5. To attain a defined pre-dilution, the generated aerosol particles were passed parallel to an adjustable and particle-free air flow into an atmospheric decoupled mixing channel. For this purpose, both flows were turbulently mixed at the channel entrance. The aerosol flow to be analysed was firstly passed through a 5.0 L compensation tank to reduce fluctuations in the PNC, which can arise e.g. by the incidence of the stick-slip-effect. Afterward, the aerosol passed a commercial dilution unit (Model VKL10, Palas GmbH, Germany) and a bipolar neutraliser (Model 3077A, TSI Inc., USA) for a further defined reduction of PNC and to improve the charge condition of the aerosols. The measuring devices received their aerosol sample through a flow splitter. The sample flow of the APS was additionally diluted by partial back-mixing with HEPA-filtered device exhaust.

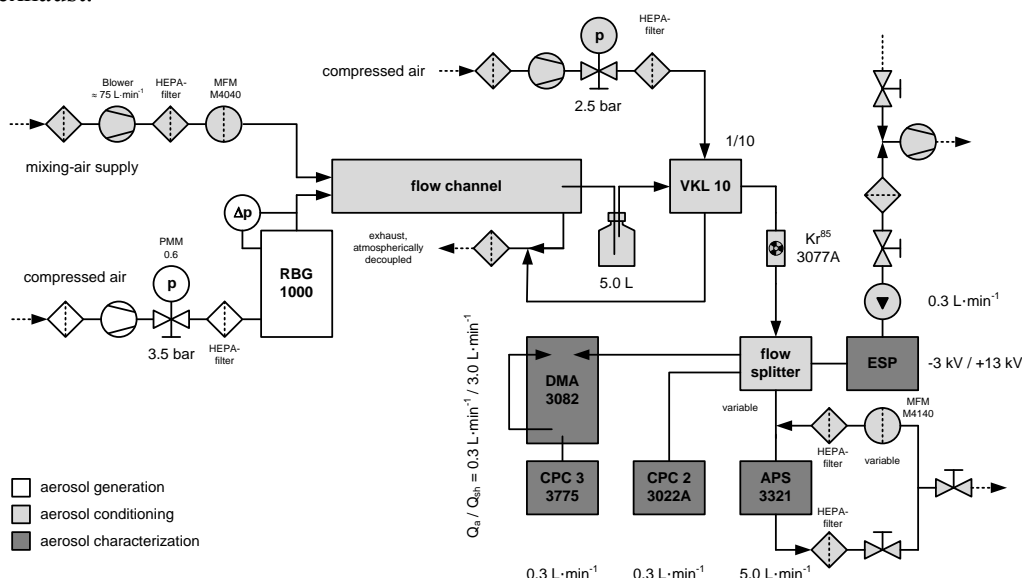


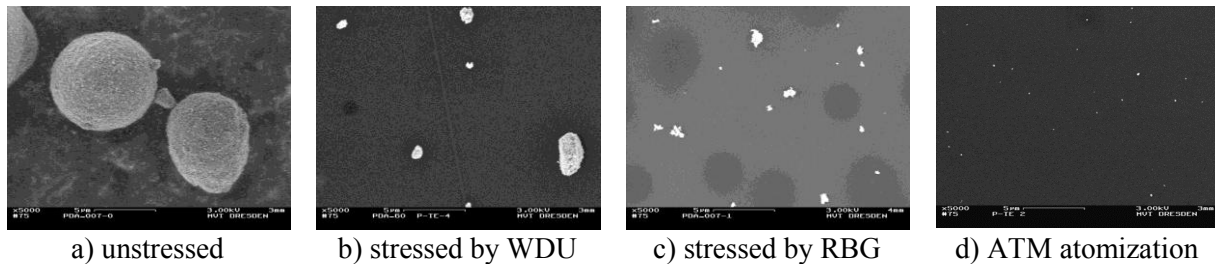
**Figure 5.** Experimental setup for intense dry powder dispersion by operating the RBG.

For the operation of the experimental setup, non-conductive tubing was installed before the neutralisers, whereas conductive tubing was used behind the neutralisers. In order to attain charge saturation of aerosol-facing components and thus to reduce particle losses and ensure maximum PNCs, the measurements were started not earlier than 60 min after feeding the RBG 1000 with a new powder sample. During the analyses, a mean relative humidity of  $19.4\% \pm 2.1\%$  and a mean temperature of  $27.9^\circ\text{C} \pm 1.7^\circ\text{C}$  were logged.

#### 4. Results for particle release for weak and intense dispersion

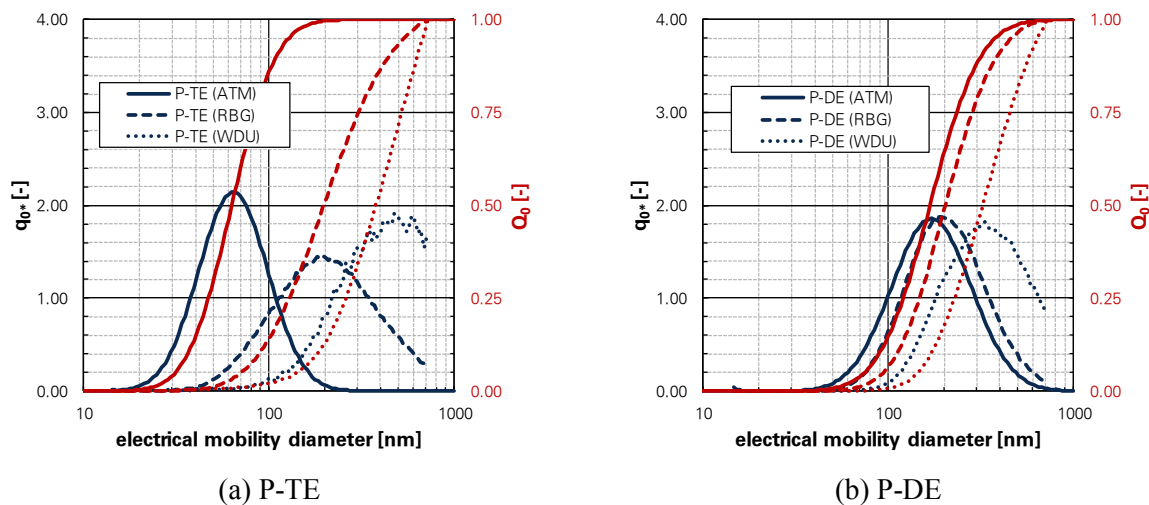
The electron microscopic images (SEM, Model Gemini 982, Karl Zeiss AG, Germany) of equal magnification given in Figure 6 show the dispersion energy impact on the agglomerate size of the nanostructured Pigment P-TE. The first image based on simple powder dusting with a brush onto a carbon-conductive tab and shows thus the “unstressed” agglomerates.

Figure 6 b and Figure 6 c show electrostatic precipitated agglomerates after the dry dispersion procedures, whereas Figure 6 d refers to the agglomerates after atomization of the ultra-sonicated suspension ( $e_{V,CAL} = 367 \text{ MJ} \cdot \text{m}^{-3}$ ). Despite the comparatively high energy input during RBG operation, released agglomerates are significantly coarser than the ones from the wet dispersion process by ultrasonication.



**Figure 6.** SEM-images of P-TE agglomerates for the different dispersion procedures; bar  $\triangleq 5 \mu\text{m}$ .

The corresponding  $\text{PSD}_0$  of P-TE and P-DE given in Figure 7 were derived solely from the SMPS-data. Results show that the dry dispersion processes (WDU, RBG) were not able to reach the  $\text{PSD}_0$  of the smallest dispersible units (based on the wet dispersion process, i.e. ATM) despite intense dispersion, immediate aerosol dilution and bipolar neutralisation.



**Figure 7.** Comparison of the  $\text{PSD}_0$  determined for the simulated dry powder dispersion procedures in comparison to the  $\text{PSD}_0$  smallest dispersible units determined by atomization (ATM) of the ultra-sonicated suspensions ( $e_{V,CAL} = 367 \text{ MJ} \cdot \text{m}^{-3}$ ).

An overview on the nanoparticle fractions and the fractions of agglomerates  $x \leq 200 \text{ nm}$  determined by SMPS during the weak and intense dry dispersion procedures for the analysed powder samples and batches are given in Figure 8.

Results show that the nanoparticle fraction does not exceed a value of 20 %. Taking into account that solely the SMPS measurement range was used for the determination of  $Q_0(100 \text{ nm})$  and  $Q_0(200 \text{ nm})$ , the quantities would be significantly lower than the determined ones by considering the whole  $\text{PSD}_0$ .

According to our previous studies regarding the particle release characterization from nanostructured materials [21, 24], fractional particle release numbers were determined from the measurement data and the analytical conditions and related to the dispersed powder sample mass.



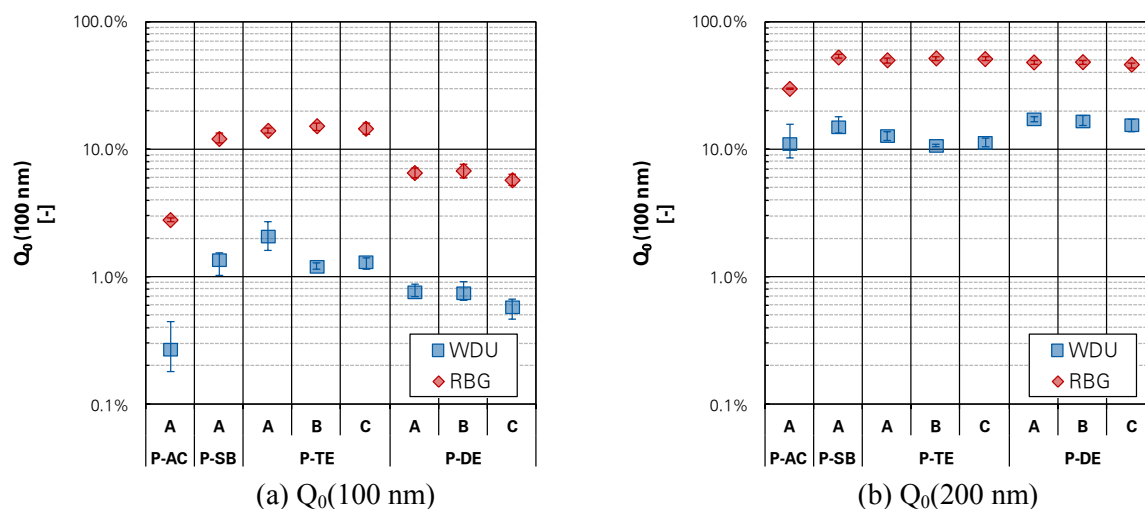


**Figure 8.** Selected number quantity-fractions based on SMPS-Data of the analysed powders and their batches, error bars = data span of 3-5 repeated dispersion procedures with at least 3 measurements.

The fractional and mass-specific numbers of released particles are given in Figure 9 for total particle release (i.e.  $x < 10 \mu\text{m}$  based on CPC-Data), the nanoparticle release (i.e.  $x < 0.1 \mu\text{m}$  based on SMPS-Data) and the micrometer particle release (i.e.  $1.0 \mu\text{m} \leq x \leq 20.0 \mu\text{m}$  based on APS-Data).

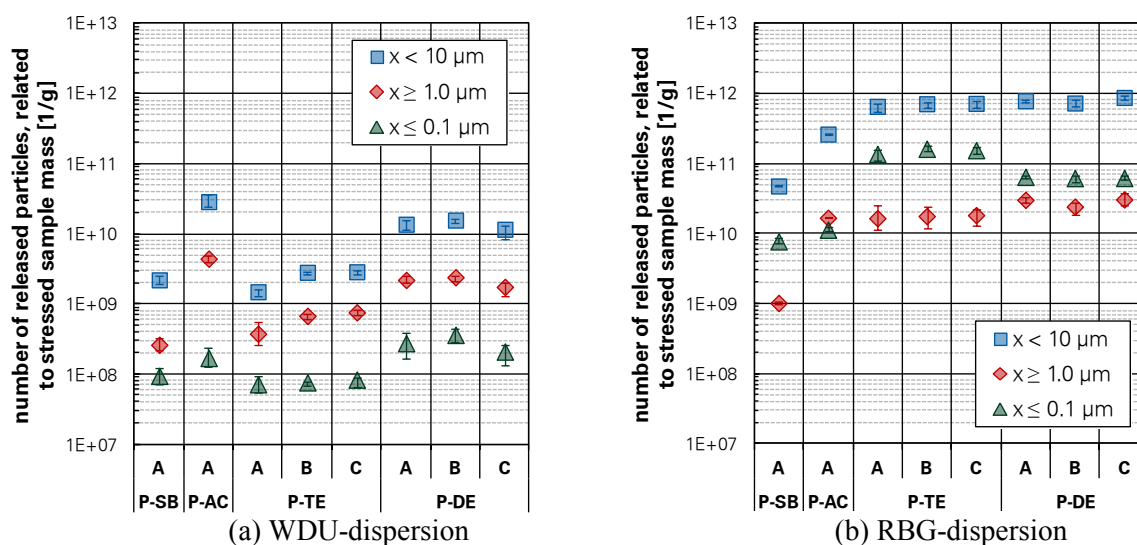


**Figure 9.** Fractional particle release numbers related to the dispersed sample mass; error bars = data span of 3-5 repeated dispersion procedures with at least 3 measurements.

Depending on the applied energy input, the particle release varied over magnitudes. For example, the simulated intense release scenario led to particle release numbers ( $x < 10 \mu\text{m}$ ) up to 400 times higher in the case of P-TE and up-to 80 times higher for P-DE in comparison to the simulated weak one. The powder sample age (i.e. comparison between the different batches A, B and C) shows a comparable minor impact on the particle release.

## 5. Summary and conclusion

The paper addressed test-scenarios for particle release from nano-structured powders, which simulates dispersion processes with low and high energy input and provides time-constant release signals. In this

context it could be shown that the relative particle velocity  $v_{rel}$  is the crucial agglomerate dispersion parameter in air flows. This set a serious limitation to the measurement technique, which can be used to study the particle release: aerosol sample feeding systems frequently expose the airborne particles to a maximum  $v_{rel}$ , which are larger than in the test-scenario, thus induce a second dispersion step, which distort the result of the particle release test. The designed “weak dispersion unit” is operated under such conditions ( $v_{rel} = 25 \text{ m}\cdot\text{s}^{-1}$ ) that post-dispersion can be excluded for most aerosol characterisation instruments. Note that for powders with sufficient flowability, the operation of some commercial aerosol generators at similar conditions is also possible. The WDU is supplemented by an “intense dispersion unit” (rotating brush generator) operated at similar powder mass flow and at  $v_{rel} = 100 \text{ m}\cdot\text{s}^{-1}$ .

The combined test-scenario for low and high energy dispersion was employed to study the particles release from two iron oxide powders (a nano-structured one and a non-nanostructured one) and two filter test powders. The results allow to conclude that the combined test-scenario yields reproducible results on particle release, clearly demonstrates the impact of energy input and facilitates the grouping of powders according to their release characteristics.

Finally, the authors would like to initiate a discussion on how to deal with the fact, that current state-of-the-art sizing instrumentation does not allow a quantitative release study for very weak dispersion energies or - more generally - implicate remarkable dispersion stress for particles to be measured.

### Acknowledgement

This work is supported by the German Federal Ministry of Economic Affairs and Energy (BMWi) under grant IGF 17785/BR/1.

### References

- [1] Kuhlbusch T A J, Asbach C, Fissan H, Göhler D and Stintz M 2011 *Part. Fibre Toxicol.* **8** 22
- [2] Schneider T and Jensen KA 2008 *Ann. Occup. Hyg.* **52** 23-34
- [3] Jensen K, Koponen I, Clausen P and Schneider T 2009 *J. Nanopart. Res.* **11** 133-46
- [4] Tsai CJ, Wu CH, Leu ML, Chen SC, Huang CY, Tsai PJ and Ko FH 2009 *J. Nanopart. Res.* **11** 121-31
- [5] Dahmann D and Monz C 2011 *Gefahrstoffe - Reinhalt. Luft* **71** 481-87
- [6] Maynard A 2002 *Ann. Occup. Hyg.* **46** 197-202
- [7] Ogura I, Sakurai H and Gamo M 2009 *J. Phys. Conf. Ser.* **170** 012003
- [8] Plitzko S, Gierke E, Dziurawitz N and Broßell D 2010 *Gefahrstoffe - Reinhalt. Luft* **70** 31-35
- [9] Stahlmecke B, Wagener S, Asbach C, Kaminski H, Fissan H and Kuhlbusch TAJ 2009 *J. Nanopart. Res.* **11** 1625-35.
- [10] Pohl M, Schubert H and Schuchmann HP 2005 *Chem. Ing. Tech.* **77** 258-62
- [11] Brenner H 1958 *The Physics of Fluids* **1** 338-46
- [12] Naue G, Liepe F, Mascheck HJ, Reher EO and Schenk R 1983 *Technische Strömungslehre I.* (Leipzig: Deutscher Verlag für Grundstoffindustrie).
- [13] Zeidan M, Xu B, Jia X and Williams R 2007 *Chem. Eng. Res. Des.* **85** 1645-54
- [14] Fuchs NA 1964 *The mechanics of aerosols* (Oxford: Pergamon Press)
- [15] Kousaka Y, Okuyama K, Shimizu A and Yoshida T 1979. *J. Chem. Eng. Jpn.* **12** 152-59.
- [16] Bagster D and Tomi D 1974 *Chem. Eng. Sci.* **29** 1773-83
- [17] Zahradnicek A 1976 *Untersuchungen zur dispergierung von Quarz- und Kalksteinfraktionen im Korngrößenbereich 0.5 - 10  $\mu\text{m}$  in strömenden Gasen.* (PhD thesis, Universität Karlsruhe)
- [18] Zahradnicek A and Löffler F 1976 *Staub - Reinhalt. Luft* **36** 425-27
- [19] Leschonski K, Röthele S and Menzel U 1984 *Part. Part. Syst. Charact.* **1** 161-66
- [20] Bürgelt T, Adam R, Rudolph A and Große S 2013 *Filtrieren und Separieren* **27** 72-77
- [21] Göhler D, Nogowski A, Fiala P and Stintz M 2013 *J. Phys. Conf. Ser.* **429** 01204
- [22] Göhler D, Stintz M, Hillemann L and Vorbau M 2010 *Ann. Occup. Hyg.* **54** 615-24
- [23] He M and Dhaniyala S 2013 *J. Aerosol Sci.* **61**, 13-26
- [24] Göhler D and Stintz M 2014 *J. Nanopart. Res.* **16** 2520